



**Universiteit  
Leiden**  
The Netherlands

## **Modeling of the cardiac sympathetic nervous system and the contribution of epicardium-derived cells**

Ge, Y.

### **Citation**

Ge, Y. (2021, December 15). *Modeling of the cardiac sympathetic nervous system and the contribution of epicardium-derived cells*. Retrieved from <https://hdl.handle.net/1887/3247258>

Version: Publisher's Version

License: [Licence agreement concerning inclusion of doctoral thesis in the Institutional Repository of the University of Leiden](#)

Downloaded from: <https://hdl.handle.net/1887/3247258>

**Note:** To cite this publication please use the final published version (if applicable).

# 7

## SINGLE-NUCLEUS RNA SEQUENCING REVEALS THE CELLULAR COMPOSITION AND MOLECULAR SIGNATURE OF MURINE SUPERIOR CERVICAL GANGLIA

Yang Ge<sup>\*1,2</sup>, H. Sophia Chen<sup>\* 1,2</sup>, Ruben Methorst<sup>2</sup>, Lieke van Roon<sup>1,2</sup>, Marco de Rooter<sup>1</sup>, Szymon M. Kielbasa<sup>3</sup>, Monique R.M. Jongbloed<sup>1,2</sup>

1. Department of Anatomy & Embryology, Leiden University Medical Center, Einthovenweg 20, 2333 ZC Leiden, The Netherlands;

2. Department of Cardiology, Leiden University Medical Center, Albinusdreef 2, 2333 ZC Leiden, The Netherlands;

3. Department of Cell and Chemical Biology, Leiden University Medical Center, Einthovenweg 20, 2333 ZC Leiden, The Netherlands;

4. Department of animal ..., Leiden University Medical Center, Albinusdreef 2, 2333 ZC Leiden, The Netherlands;

\* Authors contribute equally

Manuscript in preparation

**ABSTRACT**

The superior cervical ganglion (SCG) provides sympathetic nerve fibers to the murine anterior myocardium, an area that can be involved in large transmural myocardial infarctions. It has been shown that overactivity of SCG is associated with adverse clinical outcome after myocardial infarction. Despite these findings and a plethora of knowledge regarding electrophysiological function and histology, the exact cellular composition and molecular signature of the SCG remains to be elucidated. Here, we report a single-nuclei RNA-sequencing (snRNA-seq) study on murine SCG in order to provide an overview of its variety in cellular compositions and focused laterally and sex differences. We identified 7 major cell types, among which 5 subtypes of neuronal cells and 4 subtypes of satellite glial cells were distinguished. Assessment of potential heterogeneity between sexes revealed differences in cellular distribution and gene expression. No obvious laterality differences were detected on this healthy murine SCG dataset. Our data provides insight into the heterogenous SCG cellular composition and gene expression in a normal healthy state, thus providing a resource for further disease-oriented studies.

**Keywords**

Single-nucleus RNA sequencing, superior cervical ganglion, cellular composition, molecular signature, sex differences, laterality differences

## INTRODUCTION

The autonomic nervous system (ANS), which is divided in parasympathetic and sympathetic branches, strictly regulates multiple organ systems including the cardiovascular system [1]. Cardiac sympathetic innervation is mainly provided by nerve fibers from the bilateral superior cervical ganglia (SCG), stellate ganglia, and upper thoracic ganglia [2]. Each of these ganglia have been shown to innervate different regions of the heart [3]. The SCG projects nerve fibers to the anterior myocardium [4], an area which can be involved in large transmural myocardial infarctions after atherosclerotic occlusion of the left anterior descending coronary artery, and is regarded as a factor associated with adverse clinical outcome when overactive [5]. Upon myocardial infarction, cardiac sympathetic innervation can drastically change, with remodeling of sympathetic nerves and neurons resulting in sympathetic overdrive, which has been associated with adverse outcome in patients due to increased risk of ventricular arrhythmias [6, 7]. Changes in SCG structure and/or composition have also proven to be relevant in other diseases, such as diabetic sympathetic autonomic neuropathy and obesity [8-10].

Single-cell sequencing technologies allow for accurate exploration of the molecular signature of individual cells in complex tissues, such as sympathetic ganglia. A variety of previously unknown neuronal (sub)types in the SCG, stellate ganglia, and sympathetic chain ganglia have been identified using single-cell sequencing [11]. Similarly, different maturation and differentiation states of satellite glial cells in stellate ganglia have been identified [12]. Current literature focuses on subclassification of neuronal cells or specific non-neuronal cells in sympathetic ganglia. Although these findings are crucial to elucidate cell-type specific behavior in sympathetic ganglia, a complete outline of the cellular composition in the superior cervical ganglion is currently lacking, thus hampering interpretation of molecular changes at the single cell level in disease states.

It is hypothesized that individual healthy ganglia may already present differences in sex and laterality of the ganglia. Recently, significant transcriptomic differences between the male and female have been revealed in the left stellate ganglia in healthy adult mice [13]. Sympathetic ganglia show distinct laterality in terms of morphology (macroscopic and microscopic) and function, despite being symmetrically distributed along the paravertebral locations [14-17].

However, this classification of cellular phenotypes based on detailed molecular signatures is currently still lacking in the superior cervical ganglia. Here, we aim to provide an overview of potential sex-specific (male versus female) and side-specific (left versus right) differences of healthy adult murine SCG by assessment of heterogeneity in transcriptomic diversity at single nucleus resolution.

## MATERIAL AND METHODS

### Animals

Two female and two male C57BL/6J mice (Charles River Laboratories Inc, Wilmington, MA, USA), 15 weeks of age, were used for snRNA-seq. Animals were euthanized by CO<sub>2</sub> asphyxiation. This animal study was performed in accordance with the regulations of Animal welfare and rights in the Netherlands (The Animals Act 2011) and approved by the Animal Ethics Committee of the Leiden University Medical Center (Leiden, The Netherlands) (AVD1160020185325).

### Cell dissociation

A protocol for the methods used here is described in detail in *Chapter 6*. Briefly, bilateral superior cervical ganglia (n=8) were identified, isolated, and collected in cold Dulbecco's phosphate-buffered saline (DPBS, Gibco, Grand Island, NY, USA). Next, the individual ganglia were incubated in a 0.25% Trypsin-EDTA solution (Thermo Fisher Scientific, Waltham, MA, USA) at 37°C for 40 min in separate tubes. After removal of Trypsin, 500 µl of 1400U/ml collagenase type 2 dissolved in supplemented Neurobasal Medium (1x, Gibco, Grand Island, NY, USA; 1x B-27plus (Gibco, Grand Island, NY, USA), 2mM L-glutamine (Thermo Scientific, Waltham, MA, USA) and, 1x Antibiotic-Antimycotic (Gibco, Grand Island, NY, USA)) was added and incubated at 37°C for 40 minutes. The dissociated cells were then carefully triturated with 1 ml pipette tips. After trituration, the cell suspension was transferred into the a 15 ml tube containing 5 ml supplemented Neurobasal Medium and spun down for 10 minutes at 300 rcf at room temperature. Thereafter, the supernatant was carefully removed, and the pellet was resuspended with 270 µl fetal bovine serum (Biowest LLC, Bradenton, FL, USA). 5 µl 0.4% Trypan blue dye (Bio-Rad Laboratories, Hercules, CA, USA) was added to 5ul of each cell suspension and live cell numbers were counted using a cell counter. 30 µl Dimethyl sulfoxide (Sigma-Aldrich, Saint Louis, MO, USA) was added into each cell suspension, mixed, and transferred into cryovials. Cryovials were kept in Corning Coolcell containers (Corning Incorporated, Corning, NY, USA) at -80°C overnight and transferred into liquid nitrogen the next day until further use.

### Nucleus isolation and hashing

After thawing the cryovials at 37°C, 1 ml supplemented Neurobasal Medium was added. Each cell suspension was loaded into a MACS SmartStrainer (30 µm; Miltenyi Biotec) separately and rinsed with 5ml supplemented Neurobasal Medium. The cell suspension was centrifuged at 300 rcf for 5 minutes and supernatant was carefully removed and resuspended in 50 µl cell wash (0.04% BSA in DPBS) (Sigma-Aldrich, Saint Louis, MO, USA). Next, the cell suspension was

transferred into an Eppendorf DNA/RNA LoBind tube (EP0030108035) and centrifuged at 500 rcf for 5 minutes at 4°C. 45 µl supernatant was removed and replaced with 45 µl chilled Lysis Buffer (10 mM Tris-HCL, 10mM NaCl, 3 mM MgCl<sub>2</sub>, 0.1% Nonidet P40 Substitute, 40 U/ml RNase inhibitor (Sigma-Aldrich, Saint Louis, MO, USA) in Nuclease-Free Water (ThermoFisher Scientific, Waltham, MA, USA)). After 8 minutes of incubation on ice, 50 µl cold nuclei wash buffer was added to each tube (1xDPBS with 2% BSA and 20 U/ml RNase Inhibitor) and spun down at 600 rcf for 5 minutes at 4°C. 95 µl of supernatant was removed and 45 µl chilled Nuclei wash buffer was added to the pellet. Next, the nuclei suspension was centrifuged at 600 rcf for 5 minutes at 4°C and the supernatant was removed. 50 µl ST staining buffer (ST-SB) (10 mM Tris-HCL, 146 mM NaCl, 21 mM MgCl<sub>2</sub>, 1 mM CaCl<sub>2</sub>, 2% BSA, 0.02% Tween-20 in Nuclease-free water) was added to the nuclei pellet and resuspended carefully. 5 µl Fc Blocking reagent (Biolegend, San Diego, CA, USA) was added per 50 µl of ST-SB/nuclei mix and incubated for 10 minutes on ice. 1 µl of unique hashtag-oligos antibodies (HTO, Mab414) were added per 50 µl of ST-SB/nuclei mix to all 8 superior cervical ganglia samples and incubated for 10 minutes on ice. 100 µl of ST-SB was added to each sample and spun down for 5 minutes at 600 rcf at 4°C. 145 µl supernatant was removed and the previous step was repeated once. After removing the supernatant and resuspending the nuclei pellet in 50 µl ST-SB, nuclei were counted. Next, nuclei suspensions were centrifuged for 5 minutes at 600 rcf at 4°C and resuspended in ST-SB to reach the target nuclei concentration of 1,000-3,000 nuclei/µl for each sample and individual samples were pooled together.

### Single nuclei library preparation and sequencing

Single nuclei gene expression libraries were generated on the 10x Genomics Chromium platform using the Chromium Next GEM Single Cell 3' Library & Gel Bead Kit v3.1 and Chromium Next GEM Chip G Single Cell Kit (10x Genomics, Pleasanton, CA, USA) according to the manufacturer's protocol. TotalSeq-A hashtag libraries were generated using the Chromium Single Cell 3' Feature Barcode Library Kit (10x Genomics) according to the manufacturer's protocol. Gene expression and hashtag libraries were sequenced on a NovaSeq 6000 S4 flow cell with PE150bp sequencing using v1.5 chemistry (Illumina, San Diego, CA, USA).

### snRNA-seq data analysis

Cell Ranger software v4.0.0 (10x Genomics) was used for library demultiplexing, fastq file generation and read alignment. The resulting matrices contain the number of unique molecular identifiers (UMIs) per gene or per hashtag barcoding antibody-oligo (HTO) for each cell. Downstream analyses were performed by using R 4.0.5 and the R package Seurat (version 4.0.2, Satija Lab) [18]. Nuclei were included in analysis if passing the following criteria: i)

nFeature > 500 and nCount < 15000; ii) percent.mito < 5% and percent.RP < 3%; iii) the individual nuclei showed clear expression of a single HTO.

**Normalization** counts were normalized, scaled with default thresholds in Seurat

**Dimension reduction and clustering.** Principal component analysis was performed to identify major sources of variation within the dataset. The elbow plot was used to assess inclusion of principal components that would be used for downstream analyses. In total, 20 PCs were included. Clustering was performed with a resolution of 0.5. Dimension reduction was performed using UMAP reduction.

**Heatmaps.** Function FindVariableFeatures from Seurat was used to identify highly variable genes of the dataset. The top 500 highly variable genes were employed to generate a heatmap to show hierarchical clustering.

**Differential gene expression analysis.** Function FindAllMarkers from Seurat was used to find differential expression genes (DEGs) of each cluster by comparing the gene expression of every cluster to all remaining clusters. The list of DEGs per cluster with adjusted p-value < 0.05 (Wilcoxon rank sum test) was used for a Gene Ontology (GO) enrichment analysis using the default Kolmogorov–Smirnov test.

**Subtypes of neurons analysis.** To subcluster neurons, 13 PCs were included in clustering and dimension reduction (resolution=0.4, k.param=10). DEGs analysis of subclusters was performed with Function FindAllMarkers from Seurat.

**Subtypes of glial cells analysis.** DEGs analysis was performed with Function FindAllMarkers by comparing the gene expression of each glial cell cluster to the other glial cell clusters.

**Sex differences and bilaterality differences analysis.** Sex information and bilaterality information of each nucleus was assigned according to HTO expression. DEGs between male and female (or left versus right) were generated with Function FindMarkers from Seurat R package and GO enrichment analyses was performed on significant DEGs.

## RESULTS

### Single nucleus clustering and cell type identification of mouse SCG

Droplet-based high-throughput single nucleus RNA sequencing was performed on a HTO barcoded nuclei suspension of 8 adult murine SCG. After read quality control, alignment and quality control, a total of 4,721 high quality single nuclei were used for subsequent analysis. SCG nuclei were clustered and 12 major clusters were identified (**Fig. 1A**). There was sufficient

integration of all eight samples, indicating that differences in sample preparation were minimal (**Fig. 1B**). Next, the top 500 variably expressed genes together with the top 20 DEGs of each cluster were used to identify major cell types and clusters of similar molecular characteristics (i.e. cluster 4 and 9 as stromal cells), based on known cell markers (**Fig. 1C**, **Supplemental Fig. 1A**, **Supplemental Table 1**).

To further extrapolate cell type identity of these clusters, expression levels of multiple known marker genes for every cell type were visualized (**Figure 1C** and **Supplemental Figure 1B**): *S100b* and *Fabp7* for satellite glial cells [12]; *Tubb3* and *Th* for adrenergic neurons [19]; *Sox10* and *Ncmip* for Schwann cells [20]; *Vwf* and *Pecam1* for endothelial cells [21]; *Acta2* and *Myh11* for vascular smooth muscle cells (vSMAs) [22]; *Col1a1* and *Dcn* for stromal cells; *Ccr5* and *Cd14* for immune cells. Nuclei clustering and DEGs analysis indicated cellular heterogeneity of neuronal subtypes (cluster 6-7), satellite glial cell subtypes (cluster 0-3) and stromal cell subtypes (*Lum+* stromal cells and *Cldn1+* stromal cells) as was reported previously in other sympathetic and sensory ganglia [12, 23, 24].

In total, we identified seven major cell types in the SCG, including neuronal cells, satellite glial cells, Schwann cells, endothelial cells, smooth muscle cells, stromal cells and immune cells (**Fig. 1**).

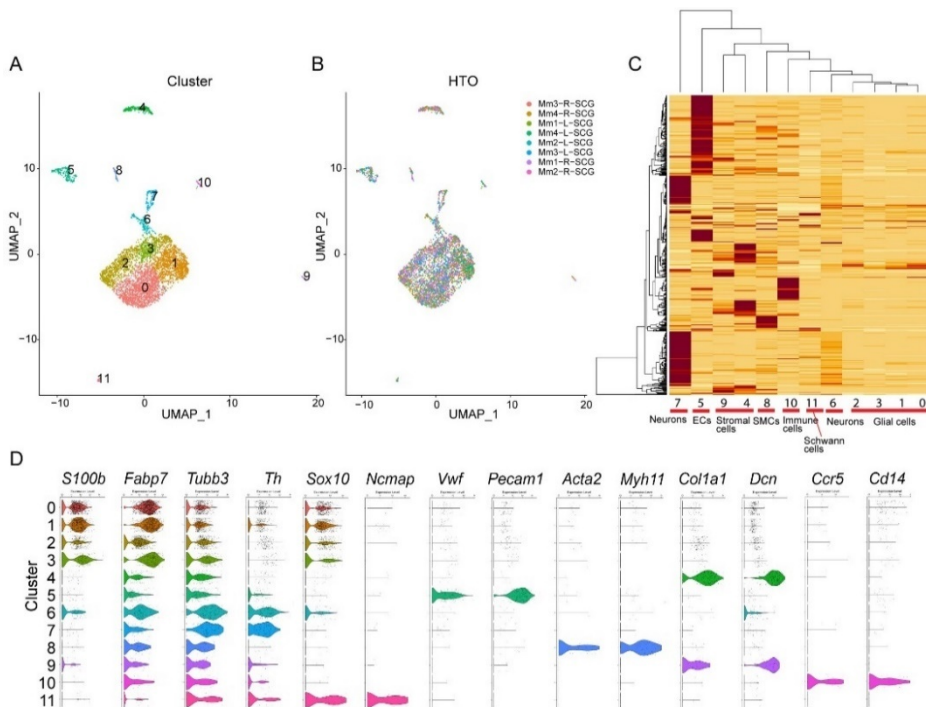


**Figure 1. Single nuclei clustering and cell type identification.** A. UMAP plot of 4,721 single nuclei with cell clusters highlighted. B. UMAP plot of single nuclei with HTO labels highlighted. C. Heatmap and hierarchical clustering based on expression of top 500 most variable genes. D. Violin plots displaying marker gene expression of known cell types for each cluster.

### Heterogeneity among mouse SCG neurons

To characterize SCG neuronal subtypes, neuron clusters were subclustered. Subclustering analysis revealed five major subtypes of neurons (3 subclusters from original cluster 6 and 2 subclusters from original cluster 7 (**Fig. 2A, B**). All neuronal subclusters were similarly represented in all eight individual samples (**Supplemental Fig. S2**). DEGs analysis of each subclusters revealed several marker genes of neuronal subtypes (**Fig. 2C**).

Almost all SCG neuronal subtypes expressed *Dbh* (Dopamine beta-hydroxylase, converting dopamine to norepinephrine) which is known to be mainly expressed in neurosecretory vesicles in sympathetic neurons [25]. *Snap25* (Synaptosomal-Associated Protein, a presynaptic plasma membrane protein involved in neurotransmitter release) showed heterogenous expression between the individual neuronal clusters [26] (**Fig. 2D**).

Recently reported marker genes in mouse thoracic ganglia were compared to marker genes in the mouse SCG. In thoracic ganglia the following neuronal subtypes were identified: 5 subtypes of nonadrenergic neurons (NA1-5), 2 subtypes of acetylcholinergic neurons (Ach1-2) and 1 type of glutamatergic neurons (Glut) [24]. We examined the expression of these published neuronal sub-type marker genes in our dataset, which revealed that only NA4 neurons are detectable in the mouse SCG (**Fig. 2E-L**). The other neuronal subpopulation in mouse SCG could not be assigned to previously known subtypes.

Differential gene expression analysis among the neuronal subclusters indicated a distinct gene expression profile of the five neuronal subclusters in SCG neurons (**Fig. 2M**) and potential distinct functions which was further suggested by Gene Ontology (GO) enrichment analysis (**Supplemental Fig. 3**). Using this approach, we identified the following neuronal subpopulations; *Apoe*<sup>+</sup> neurons, *Kcnq1*<sup>+</sup>/*Nrg3*<sup>+</sup> neurons, *Kcnq1*/*Nrg3*<sup>+</sup> neurons, *Map1b*<sup>+</sup> neurons and *Chl1*<sup>+</sup> neurons. Ultimately, our findings are indicative of cellular heterogeneity of nonadrenergic neurons in the SCG.

### Heterogeneity of mouse SCG satellite glial cells

The important function of glial cells in the central nervous system (CNS) has been recognized for decades [27]. Although the relevance of glial cells in the peripheral nervous system has also been getting more awareness recently, still little is known about glial cells in the sympathetic ganglia [28]. Recently the presence of satellite glial subtypes with different functions have

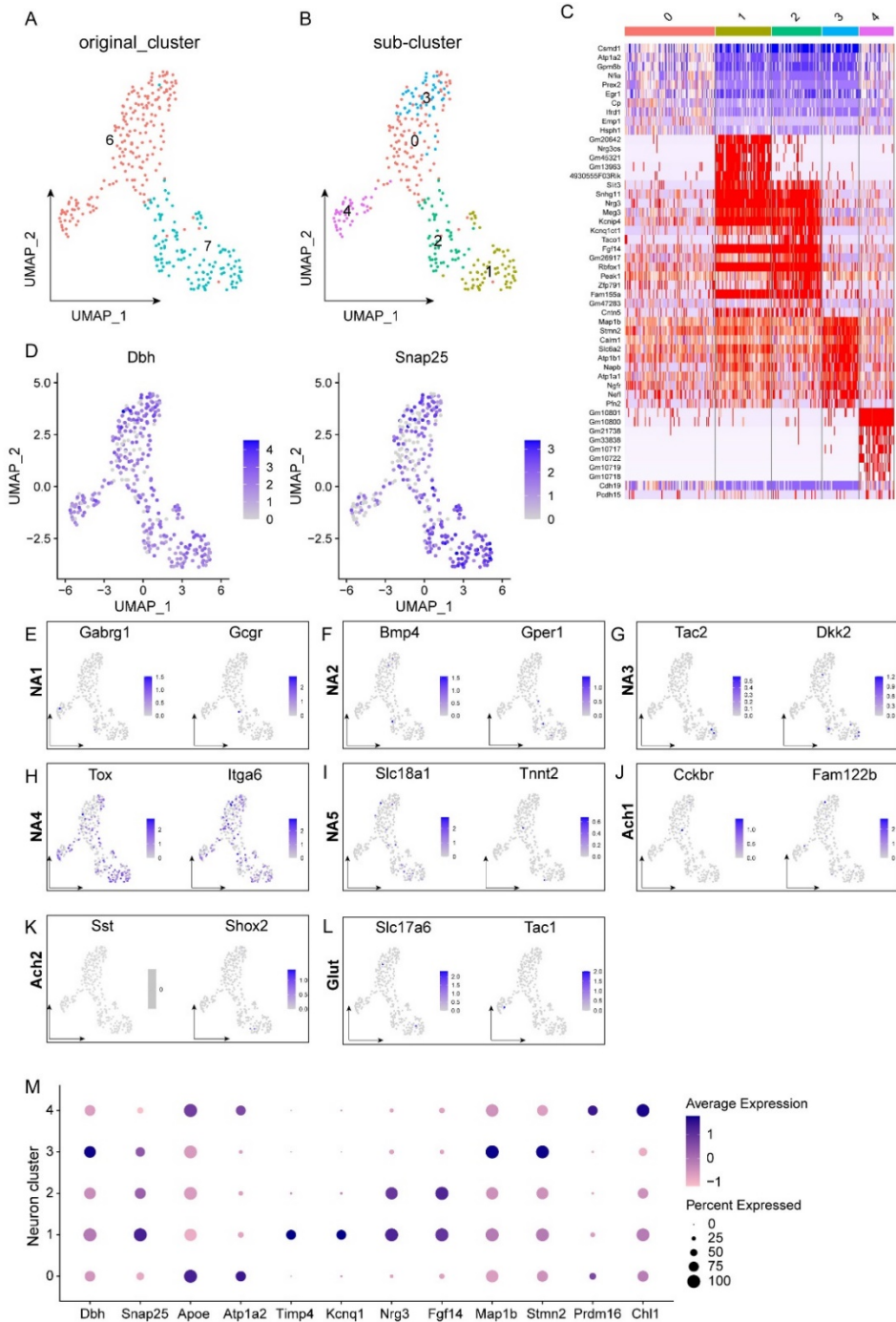


Figure 2. Identification of neuronal subtypes and markers of mouse SCG neurons. A. UMAP plot of 316

neuronal cells grouped by original cell clustering. B. Subclustering of 316 neuronal cells shown in A resulted in 5 cellular subtypes. C. Heatmap of top 10 DEGs of each neuronal subcluster. D. Overview of a well-known adrenergic neuron marker (*Dbh*) and synapse marker (*Snap25*) of neuronal clusters. E-L. Dermination of previously published neuronal subtypes with UMAP expression plots: E-I. Subtypes of adrenergic sympathetic neurons; J-K. cholinergic neurons and L. glutamatergic neurons. M. Expression of marker genes identified using subclustering of mouse SCG neuronal cells.

been identified, although their precise role is still unclear [23]. General markers for satellite glial cells (*Fabp7* and *S100b*) are currently used as the main identifiers for satellite glial cells in the peripheral nervous system. To facilitate the analysis of SCG satellite glial cells, satellite glial cells (cluster 0-3) were extracted from the whole dataset with the original clustering signatures (Fig. 3A) using *Fabp7* and *S100b*. All satellite glial sub-clusters were similarly represented over all eight individual samples (Supplemental Fig. 4). Differential gene expression analysis among the glial clusters revealed their distinct gene expression patterns (Fig. 3B). The expression of known sympathetic- and sensory-specific glial markers [23] were assessed in SCG (Fig. 3C-E). Consistent with previous findings [23], only sympathetic-specific, but almost no sensory-specific, satellite glial cells were present in murine SCG (Fig. 3C, D). General cell type gene markers of the satellite glial cells generally expressed in the peripheral nervous system, were examined in SCG as shown in Figure 3E. Results revealed that while expression of common satellite glial cells markers is present in all glial subtypes, enrichment of these markers vastly differs. Marker gene identification and GO pathway analysis of glial subclusters revealed the potential different functions of the different satellite glial cells: immuno-responsive satellite glial cells (cluster 0), which are enriched with genes such as *Junb*, *Irf1* and *Cxcl10*; fatty acid metabolic-enriched *Ptprz1*<sup>+</sup> satellite glial cells (cluster 1); migration-enriched *Ntrk3*<sup>+</sup> satellite glial cells (cluster 2) and *Dbi/Tuba1a*-enriched satellite glial cells (cluster 3) (Fig. 3F, Supplemental Fig. 5).

Glial cells are considered to communicate with other glial cells and neighbouring neurons via gap junctions. They also have a role in supporting neurons after injury, showing alterations in expression of gap junctions in response to injury [28-30]. A variety of gap junctions and other gene markers which are known to be enriched in the CNS and sensory ganglia were examined. *Cdh19* and *Sox10* are enriched in SCG satellite glial cells, while *Gfap* which is known to be highly enriched in the CNS [31], is absent in healthy mouse SCG glial cells (Fig. 4). Potassium channel protein *Kcnj10* was mainly expressed in cluster 0 and 1 of SCG glial cells (Fig. 4). Different from *Gja1* as the main type of gap junction found in sensory glial cells, SCG satellite glial cells exclusively expressed *Gjc3* in all subclusters (Fig. 4). Moreover, we found SCG satellite glial cells to express the ATP purinergic receptor *P2rx7*, which was enriched in cluster 0 and 2 (Fig. 4). Thus, we identified heterogeneity in gap junction, ion channel, and receptor expression between different glial cell subtypes, indicating that different glial cell populations may play a different role in sympathetic innervation. Moreover, we observed NGF receptor (*Ngfr*)

expression in all SCG satellite glial cells which indicates their neurotrophic factor-responsive property (Fig. 4).

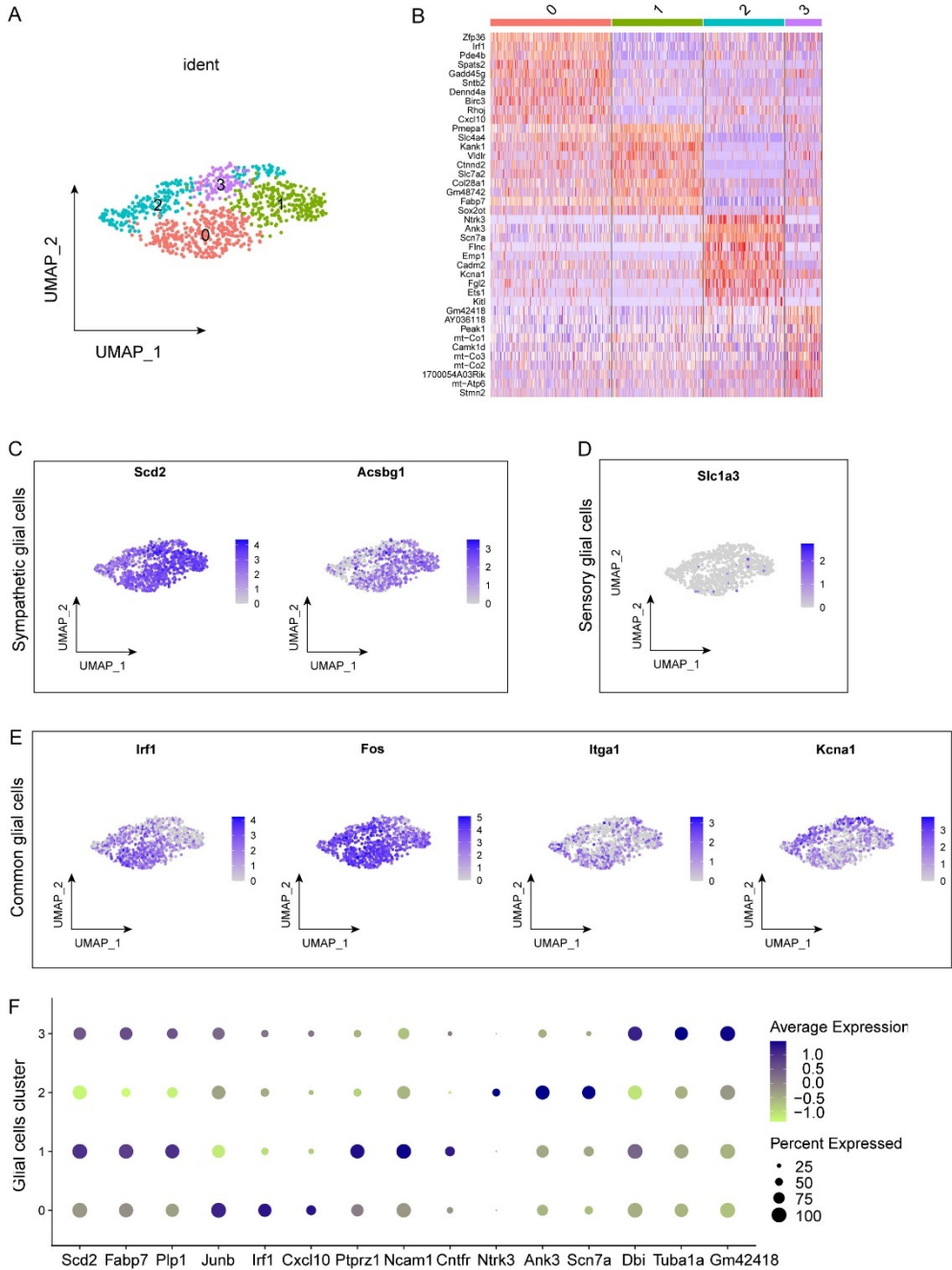


Figure 3. Identification of cellular subtypes and markers of SCG satellite glial cells. A. UMAP plot of 933 glial cells. B. Heatmap of top 10 DEGs of each glial cell population. C. Feature plot overview of two known markers of the sympathetic ganglion-specific glial cells (*Scd2* and *Acsbg1*). D. Feature plot overview of a known marker of the sensory ganglion-specific glial cells (*Sc11a3*). E. Feature plots of previously published common glial cell markers. F. Expression of marker genes of mouse SCG glial cells.

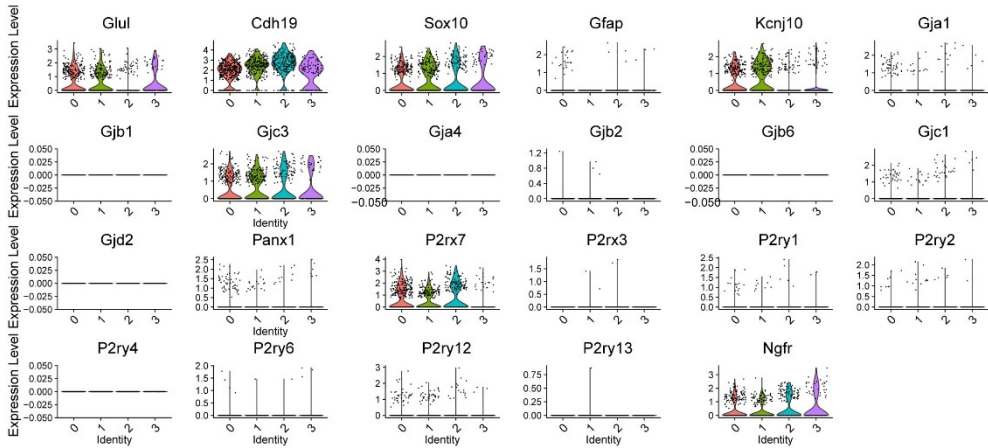


Figure 4. Mouse SCG glial cells have distinct gene expression from CNS and sensory ganglionic glial cells. Violin plots displaying expression of known CNS and sensory ganglionic glial cell marker genes in SCG glial cells.

**snRNA-seq reveals sex differences in cellular distribution and gene expression of satellite glial cells in the SCG**

Sex differences have received close attention in recent years and have been revealed in both health and disease in multiple organs/systems [32-34]. To date, a few studies of mouse and rat stellate ganglia based on bulk RNA sequencing have indicated transcriptomic differences between male and female [35, 36], however no molecular differences between sexes have been reported at single cell level. In the current study, we performed further analysis of SCG snRNA-seq data to detect molecular differences between male and female at single cell level. Single nuclei were annotated with sex information according to HTO labelling (Fig. 5A). The percentage of the nucleus numbers in each cluster/total nucleus number (to correct for differences in cell size of the different clusters) of corresponding sex was separately calculated and compared (Fig. 5B). The results indicate sex difference in cellular distribution in the mouse SCG, especially in the satellite glial cells (cluster 0-2). Differential gene expression analysis of satellite glial cells and neurons further demonstrated transcriptomic differences in satellite glial cells (cluster 0-3) between male and female, however no sex difference was detectable in neuronal clusters (Clusters 6 and 7, except for X-linked gene *Xist*) (Fig. 5C).

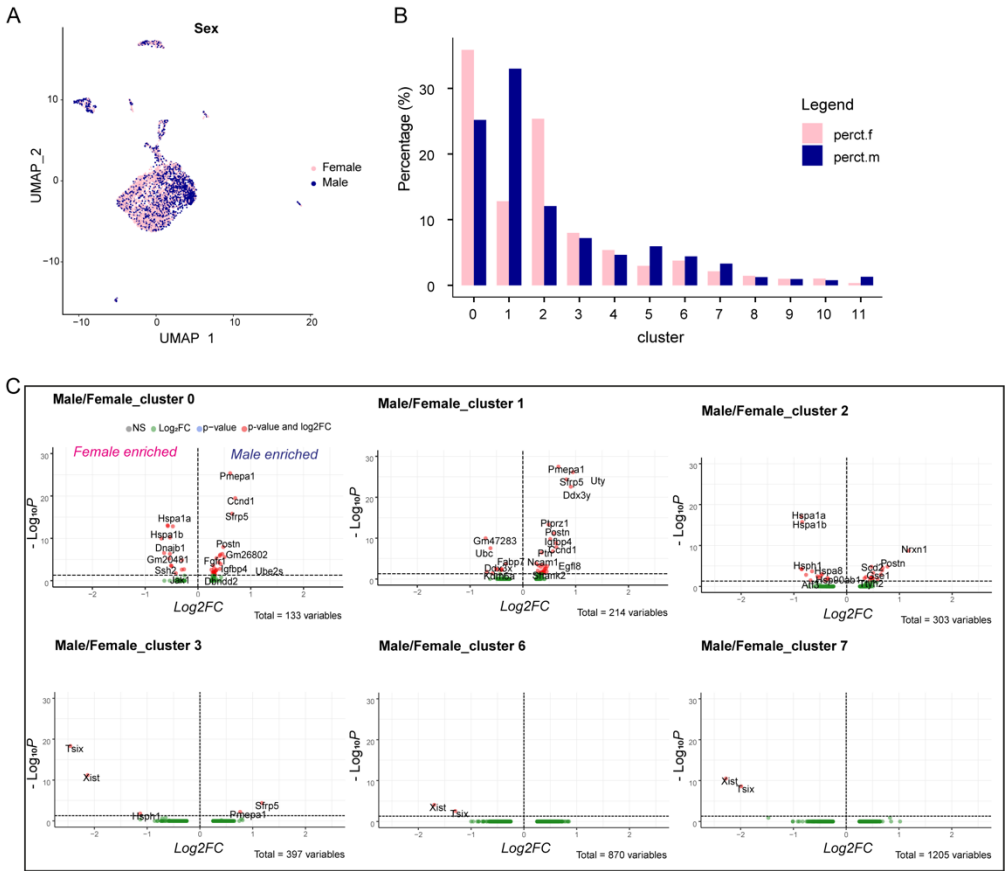


Figure 5. Sex difference analysis of mouse SCG cells. A. UMAP plot of mouse SCG cells colored by sex. B. Bar plot parallely showing cellular distribution in male and female SCG. Percentage = # nuclei per cluster / # of total nuclei. C. Volcano plot showing differentially expressed genes between male and female SCG satellite glial cells and neurons.

**Examination of potential sidedness differences in cellular distribution or gene expression of murine SCG cells**

Left and right sympathetic ganglia are known to unevenly innervate different regions of an organ or tissue, e.g. left dominant innervation of the posterior regions of ventricles by stellate ganglia [3]. The underlying molecular signatures driving these laterality differences are unknown and remains to be investigated.

To compare left and right mouse SCG, all sequenced nuclei were assigned with their laterality identification according to HTO labelling (Fig. 6A), wherafter cellular composition of the left and right SCG was determined and compared (Fig. 6B). Results revealed no obvious sidedness

differences in cellular distribution. Differential gene expression analysis of satellite glial cells and neurons indicated minor transcriptomic differences only in Junb<sup>+</sup> satellite glial cells between left and right SCG (Fig. 6C). The results suggest no obvious differences between left and right SCG in a healthy state.

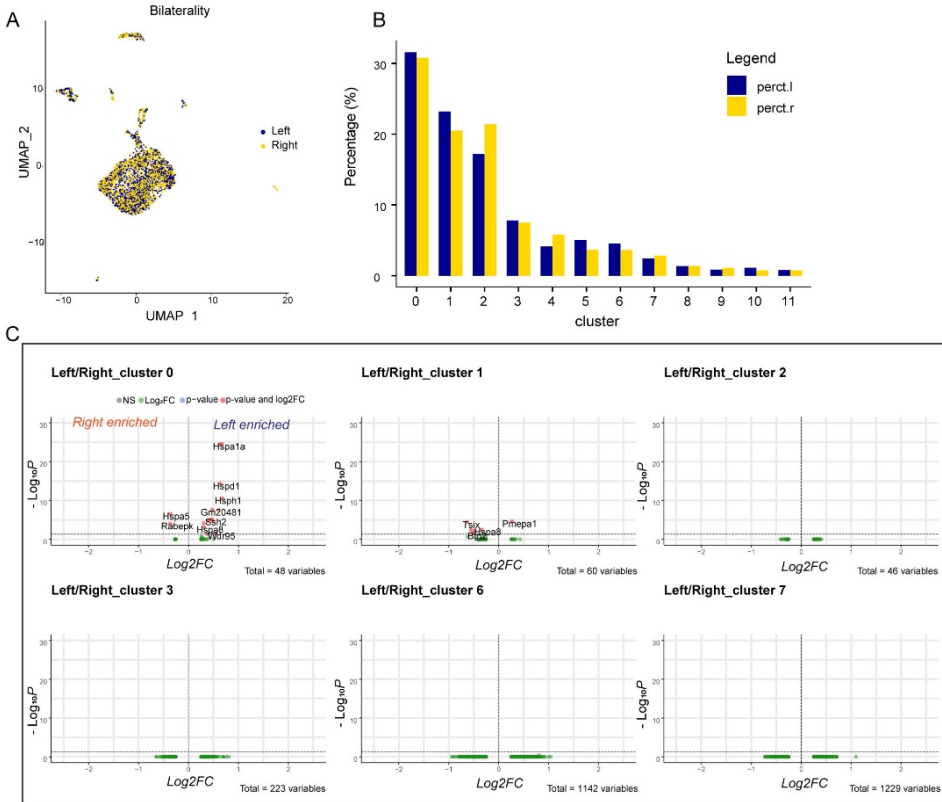


Figure 6. Sidedness analysis of mouse SCG cells. A. UMAP plot of mouse SCG cells coloured by bilaterality identification. B. Bar plot parelly showing cellular cluster distribution in left and right SCG. Percentage = # nuclei in cluster / # total nuclei. C. Volcano plot showing differentially expressed genes between left and right SCG satellite glial cells and neurons.

**DISCUSSION**

Superior cervical ganglia are important components of the cardiac sympathetic nervous system. We have previously demonstrated neuronal cell remodeling in the SCG after MI [Chapter 5]. It is well-known that ganglia are mainly composed of neuronal cells with surrounding glial cells (the majority of which are satellite glial cells), and the emerging importance of glial cells in ganglia has been recently been made aware [28, 37]. However, due

to the lack of a clear molecular signature of glial cell populations in the SCG, characterization of glial cells was not included in our previous study [Chapter 5]. In the current study, we performed snRNA-seq of healthy SCG and aimed to create a reference of the cellular composition and to identify the molecular characteristics of neuronal and satellite glial cells at healthy baseline, which can be further utilized for disease investigation.

We identified seven major cell types in the SCG, including 1). neuronal cells; 2). satellite glial cells; 3). Schwann cells; 4). endothelial cells; 5). smooth muscle cells; 6). fibroblast cells 7). stromal cells and 8). immune cells. The general cellular composition of SCG is similar to the composition of other sympathetic ganglia and sensory ganglia, however SCG display obvious differences especially in molecular signatures of neuronal cells and satellite glial cells.

**Neurons in SCG.** Furlan and colleagues have shown adrenergic, cholinergic and glutamatergic neurons in the mouse stellate ganglion [24]. However, only adrenergic neurons were detected in SCG, which indicates that the SCG biologically differs from the stellate ganglion. Of note, histological analysis of SCG did reveal cells with a cholinergic phenotype in the SCG [chapter 5]. In this regard, it is striking that we did not find these cells in our snRNA-seq data consistent with previous finding of no cholinergic neurons by single cell RNA sequencing [23]. A potential explanation might be: i) We used high throughput droplet-based 10X Genomics Chromium approach which has limited ability to detect especially low abundance transcripts [38]; ii) Previous studies, including ours, are mostly based on immune-histological staining of cholinergic markers (i.e. choline acetyltransferase), cross reaction with other proteins might happen. Studies including PCR or sequencing with Smartseq2 will be required for further exploration.

Our snRNA-seq analysis identified five distinct subtypes of adrenergic neurons in the SCG. Several noteworthy marker genes were found. Synaptosome Associated Protein 25 (*Snap25*) which is a presynaptic plasma membrane protein and plays an important role in the synaptic function in the neuronal system [26]. *Kcnq1* encodes a voltage-gated potassium channel, which regulates neuronal excitability and contributes to dysregulation of cardiac function in cases with genetic mutations [39, 40]. Among SCG neurons, cluster 1 neurons exhibited high expression of *Snap25* and *Kcnq1*, which might indicate that they are actively synaptic-coupled neurons in the SCG. Cluster 3 neurons showed high expression of *Dbh* which is required in adrenergic neurons to convert dopamine to neurotransmitter norepinephrine. This cluster of neurons also showed a high expression of Tyrosine hydroxylase (*Th*). Previous work showed that Th<sup>+</sup> neurons are situated at the outer region of SCG as was observed with immunostaining [Chapter 5]. Moreover, we also found that this cluster of neurons have high expression of *Map1b* and *Stmn2* which are necessary for the stability of neuronal microtubules and normal axonal outgrowth and regeneration [41, 42]. Interestingly, cluster 0 and 4 neurons displayed

a high expression of Brain-type fatty acid-binding protein 7 (*Fabp7*). *Fabp7* is usually considered as a glial cell marker, however, it was also previously found in neural stem cells and brain neural precursors [43, 44]. This might suggest the existence of neural precursor cells in adult mouse SCG, although further investigation is needed to substantiate this.

**Satellite glial cells in SCG.** With snRNA-seq analysis, we detected four major subtypes of satellite glial cells in mouse SCG. To have a brief understanding of these satellite cells, we used glial cells of the CNS and sensory ganglia as guidance for our cell type characterization, since more is known about these CNS and sensory glial cells compared to sympathetic ganglia. Cluster 0 satellite cells exhibited a clearly distinct expression of the transcript factor *Junb*, interferon-inducible gene *Irf1* and antimicrobial gene *Cxc10*. GO analysis demonstrated their distinct enrichment in immune-responsive pathways, which endows the similarity functions of this cluster of glial cells to microglial cells in the CNS [45, 46]. Cluster 1 satellite glial cells, showing high expression of *Ptprz1* and *Ncam*, are enriched in the pathways involving ensheathment of neurons and axons. Astrocytes and oligodendrocytes are the glial cells in the CNS with an established function in supporting neurons by their ensheathment [47, 48]. The molecular and functional similarity between cluster 1 satellite glial cells and these CNS glial cells however needs further biological validation. Remarkably, cluster 2 glial cells expressed the lowest level of *Fabp7* and exclusively expressed neurotrophin binding receptor *Ntrk3* and *Ank3* (originally found at initial segment axons and nodes of Ranvier [49]). Combined with GO analysis, cluster 2 glial cells might thus be involved in stimulation by neurotrophin and supporting axon development. The molecular print of cluster 3 glial cells is currently unclear, although a high expression of *Dbi*, *Tuba1a* and *GM42418* was detected with snRNA-seq. Furthermore, our results reveal enrichment of gap junction *Gjc3*, instead of *Gja1* that is found in CNS and sensory ganglionic glial cells. SCG satellite glial cells also express purinergic ATP receptor *P2rx7* and nerve growth factor receptor *Ngfr*.

**Sex differences in mouse SCG.** Baleys and colleagues have previously reported sex differences of mouse sympathetic ganglia with bulk RNA-seq technology [35]. However, the analysis of total mRNA extracted from whole tissue may lead to the loss of information, especially of low-enriched cells. Furthermore, it carries a risk of inclusion data of cell types that are not related to the SCG due to imprecise SCG isolation, e.g. cells from the carotid artery or carotid body that lie in close proximity to the SCG. Our snRNA-seq data elucidates the advantages that even low enriched neurons and other cell types can be extracted and analyzed separately to avoid information bias. The current snRNA-seq analysis also revealed sex differences of the SCG as was found with bulk RNA-seq [35], however differences were mainly detected in satellite glial cells, and not in neuronal cells. Moreover, by performing snRNA-seq, we could outline the

distribution of the different cell types in the SCG and, to our knowledge, these results are the first showing sex differences in the SCG at the single nucleus level.

**Sidedness of mouse SCG.** Asymmetry in cardiac innervation is widely recognized and left and right stellate ganglia show a regionalized distribution of their area of coverage [3]. Therefore in the current study, a comparison of bilateral ganglia was performed to evaluate whether SCG show laterality differences at transcriptomic level. Results indicated only minor differences in a single cluster of satellite glial cells, but no noticeable differences of SCG with respect to cellular distribution. Although no obvious laterality differences were shown at healthy conditions, it would be of interest to evaluate whether cardiac injury would cause differential changes of gene expression and cellular distribution in SCG. We strive to take the influence of cardiac damage into account in our future studies.

In summary, snRNA-seq endowed us the ability to identify the cellular composition and molecular signature of murine SCG in the healthy state. Cellular heterogeneity and subtypes of neuronal cells and satellite glial cells were revealed in healthy mouse SCG, although further biological validation is mandatory. The data of the current study provides a reference baseline to further investigate SCG remodeling at single nucleus resolution, including sex-specific and bilaterality-specific responses to cardiovascular disease.

### Limitations of the study

Sample size was limited due to a variety of factors. Subclustering of neurons was performed on a limited amount of cells in some of the subclusters. This can explain difficulties to properly characterize neuronal and glial cell subtypes based on cellular pathways, unique gene expression markers, and cellular composition. Histological and/or electrophysiological validation is necessary to elucidate the actual role of identified subtypes of neuronal cells and glial cells.

### DISCLOSURES

The authors have nothing to disclose.

### FUNDING

This work is supported by the Netherlands Organization for Scientific Research (NWO) [016.196.346 to M.R.M.J.].

### ACKNOWLEDGEMENTS

We thank Conny van Munsteren (Department of Anatomy and Embryology, LUMC, Leiden, the Netherlands) for her help in the arrangement of experimental animals and tissue preparation. We thank Susan L. Kloet (Department of Human Genetics, LUMC, Leiden, the Netherlands) for her help in experimental design and useful discussions. We thank Emile J. de Meijer (Department of Human Genetics, LUMC, Leiden, the Netherlands) for the help with single-nucleus RNA isolation and library preparation for sequencing.

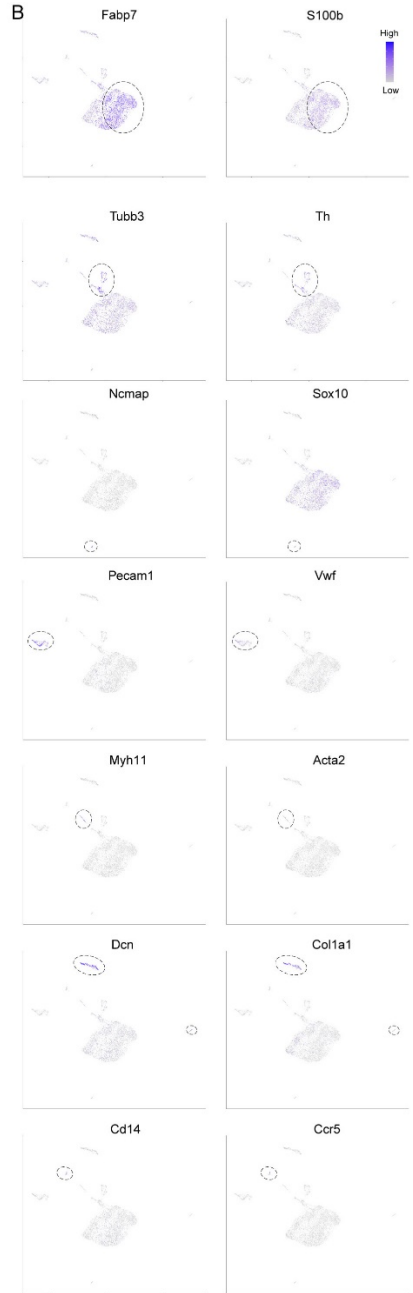
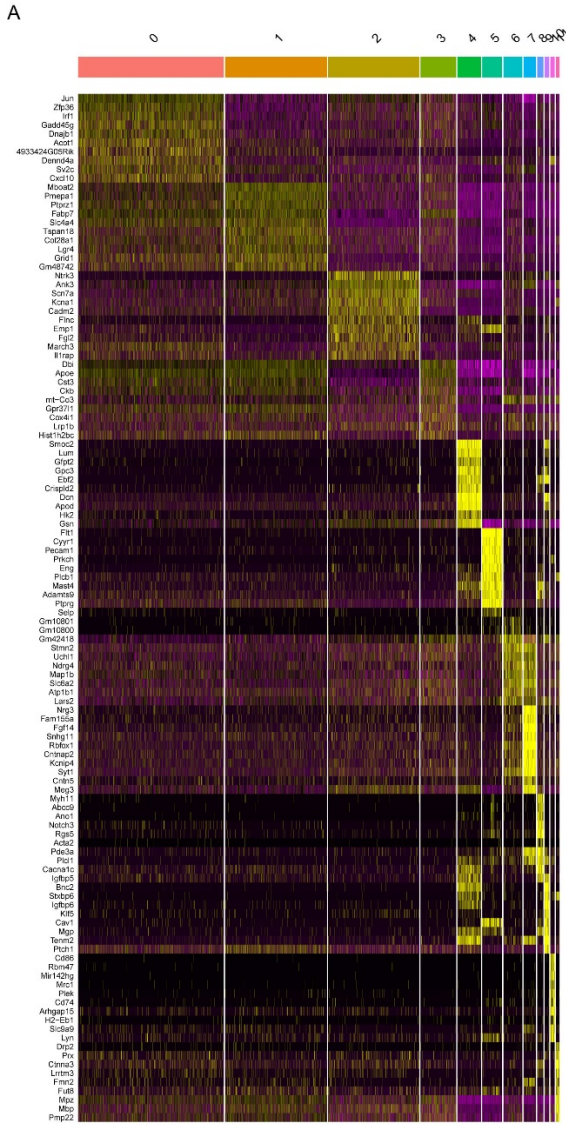
### REFERENCES

1. McCorry, L.K., *Physiology of the autonomic nervous system*. Am J Pharm Educ, 2007. 71(4): p. 78.
2. Wink, J., et al., *Human adult cardiac autonomic innervation: Controversies in anatomical knowledge and relevance for cardiac neuromodulation*. Auton Neurosci, 2020. 227: p. 102674.
3. Zandstra, T.E., et al., *Asymmetry and Heterogeneity: Part and Parcel in Cardiac Autonomic Innervation and Function*. Frontiers in Physiology, 2021. 12(1569).
4. Manousiouthakis, E., et al., *Venous endothelin guides sympathetic innervation of the developing mouse heart*. Nat Commun, 2014. 5: p. 3918.
5. Stone, P.H., et al., *Prognostic significance of location and type of myocardial infarction: independent adverse outcome associated with anterior location*. J Am Coll Cardiol, 1988. 11(3): p. 453-63.
6. Li, C.Y. and Y.G. Li, *Cardiac Sympathetic Nerve Sprouting and Susceptibility to Ventricular Arrhythmias after Myocardial Infarction*. Cardiol Res Pract, 2015. 2015: p. 698368.
7. Oh, Y.S., et al., *Spatial distribution of nerve sprouting after myocardial infarction in mice*. Heart Rhythm, 2006. 3(6): p. 728-36.
8. Stefanidis, A., et al., *Insights into the neurochemical signature of the Innervation of Beige Fat*. Mol Metab, 2018. 11: p. 47-58.
9. Li, G., et al., *Co-expression changes of lncRNAs and mRNAs in the cervical sympathetic ganglia in diabetic cardiac autonomic neuropathic rats*. J Neurosci Res, 2017. 95(8): p. 1690-1699.
10. Carroll, S.L., et al., *Ganglion-specific patterns of diabetes-modulated gene expression are established in prevertebral and paravertebral sympathetic ganglia prior to the development of neuroaxonal dystrophy*. J Neuropathol Exp Neurol, 2004. 63(11): p. 1144-54.
11. Furlan, A., et al., *Visceral motor neuron diversity delineates a cellular basis for nipple- and pilo-erection muscle control*. Nat Neurosci, 2016. 19(10): p. 1331-40.
12. van Weperen, V.Y.H., et al., *Single-cell transcriptomic profiling of satellite glial cells in stellate ganglia reveals developmental and functional axial dynamics*. Glia, 2021. 69(5): p. 1281-1291.
13. Bayles, R.G., et al., *Sex differences in sympathetic gene expression and cardiac neurochemistry in Wistar Kyoto rats*. PLoS One, 2019. 14(6): p. e0218133.
14. Kwon, O.J., et al., *Morphological Spectra of Adult Human Stellate Ganglia: Implications for Thoracic Sympathetic Denervation*. Anat Rec (Hoboken), 2018. 301(7): p. 1244-1250.
15. Wang, F.B., et al., *Axons of Passage and Inputs to Superior Cervical Ganglion in Rat*. Anat Rec (Hoboken), 2018. 301(11): p. 1906-1916.
16. Meijborg, V.M.F., et al., *Stellate ganglion stimulation causes spatiotemporal changes in ventricular repolarization in pig*. Heart Rhythm, 2020. 17(5 Pt A): p. 795-803.
17. Zhou, W., et al., *Effect of stellate ganglia stimulation on global and regional left ventricular function as assessed by speckle tracking echocardiography*. Am J Physiol Heart Circ Physiol, 2013. 304(6): p. H840-7.

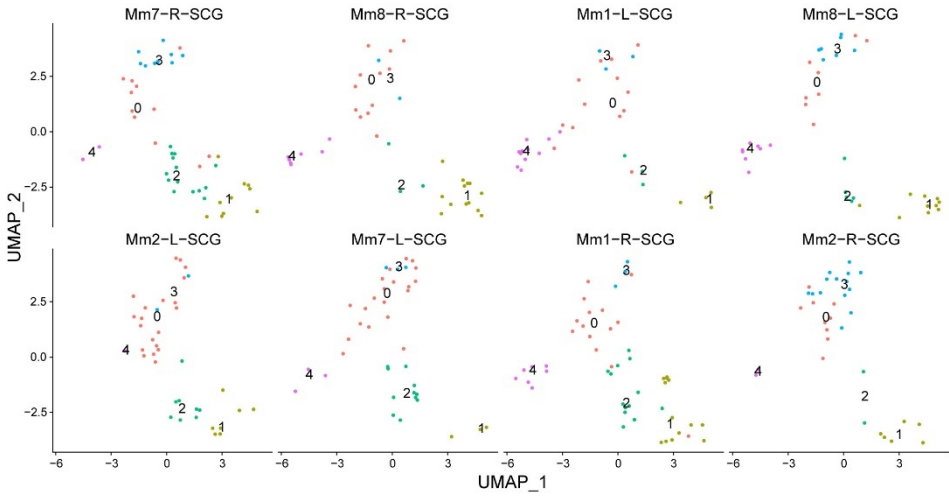
18. Stuart, T., et al., *Comprehensive Integration of Single-Cell Data*. Cell, 2019. 177(7): p. 1888-1902 e21.
19. Gervasi, N.M., et al., *The local expression and trafficking of tyrosine hydroxylase mRNA in the axons of sympathetic neurons*. Rna, 2016. 22(6): p. 883-95.
20. Finzsch, M., et al., *Sox10 is required for Schwann cell identity and progression beyond the immature Schwann cell stage*. J Cell Biol, 2010. 189(4): p. 701-12.
21. Goncharov, N.V., et al., *Markers of Endothelial Cells in Normal and Pathological Conditions*. Biochemistry (Moscow), Supplement Series A: Membrane and Cell Biology, 2020. 14(3): p. 167-183.
22. Milewicz, D.M., et al., *Altered Smooth Muscle Cell Force Generation as a Driver of Thoracic Aortic Aneurysms and Dissections*. Arteriosclerosis, Thrombosis, and Vascular Biology, 2017. 37(1): p. 26-34.
23. Mapps, A.A., et al., *Diversity of satellite glia in sympathetic and sensory ganglia*. bioRxiv, 2021: p. 2021.05.25.445647.
24. Furlan, A., et al., *Visceral motor neuron diversity delineates a cellular basis for nipple- and pilo-erection muscle control*. Nature Neuroscience, 2016. 19(10): p. 1331-1340.
25. Ernsberger, U., et al., *The expression of dopamine beta-hydroxylase, tyrosine hydroxylase, and Phox2 transcription factors in sympathetic neurons: evidence for common regulation during noradrenergic induction and diverging regulation later in development*. Mech Dev, 2000. 92(2): p. 169-77.
26. Gibbins, I.L., et al., *Heterogeneous expression of SNAP-25 and synaptic vesicle proteins by central and peripheral inputs to sympathetic neurons*. J Comp Neurol, 2003. 459(1): p. 25-43.
27. Allen, N.J. and D.A. Lyons, *Glia as architects of central nervous system formation and function*. Science (New York, N.Y.), 2018. 362(6411): p. 181-185.
28. Hanani, M. and D.C. Spray, *Emerging importance of satellite glia in nervous system function and dysfunction*. Nature Reviews Neuroscience, 2020. 21(9): p. 485-498.
29. Ji, R.R., C.R. Donnelly, and M. Nedergaard, *Astrocytes in chronic pain and itch*. Nat Rev Neurosci, 2019. 20(11): p. 667-685.
30. Huang, T.-Y., V. Belzer, and M. Hanani, *Gap junctions in dorsal root ganglia: Possible contribution to visceral pain*. European Journal of Pain, 2010. 14(1): p. 49.e1-49.e11.
31. Hol, E.M. and M. Pekny, *Glial fibrillary acidic protein (GFAP) and the astrocyte intermediate filament system in diseases of the central nervous system*. Curr Opin Cell Biol, 2015. 32: p. 121-30.
32. Klein, S.L. and K.L. Flanagan, *Sex differences in immune responses*. Nature Reviews Immunology, 2016. 16(10): p. 626-638.
33. Mecklenburg, J., et al., *Transcriptomic sex differences in sensory neuronal populations of mice*. Scientific Reports, 2020. 10(1): p. 15278.
34. Lam, C.S.P., et al., *Sex differences in heart failure*. European Heart Journal, 2019. 40(47): p. 3859-3868c.
35. Bayles, R.G., et al., *Transcriptomic and neurochemical analysis of the stellate ganglia in mice highlights sex differences (vol 8, 8963, 2018)*. Scientific Reports, 2019. 9.
36. Bayles, R.G., et al., *Sex differences in sympathetic gene expression and cardiac neurochemistry in Wistar Kyoto rats*. Plos One, 2019. 14(6).
37. Blackburn, D., et al., *Astrocyte function and role in motor neuron disease: a future therapeutic target?* Glia, 2009. 57(12): p. 1251-64.
38. Wang, X., et al., *Direct Comparative Analyses of 10X Genomics Chromium and Smart-seq2*. Genomics, Proteomics & Bioinformatics, 2021.

39. Goldman, A.M., et al., *Arrhythmia in heart and brain: KCNQ1 mutations link epilepsy and sudden unexplained death*. *Sci Transl Med*, 2009. 1(2): p. 2ra6.
40. Liin, S.I., R. Barro-Soria, and H.P. Larsson, *The KCNQ1 channel - remarkable flexibility in gating allows for functional versatility*. *The Journal of physiology*, 2015. 593(12): p. 2605-2615.
41. González-Billault, C., et al., *A role of MAP1B in Reelin-dependent neuronal migration*. *Cereb Cortex*, 2005. 15(8): p. 1134-45.
42. Klim, J.R., et al., *ALS-implicated protein TDP-43 sustains levels of STMN2, a mediator of motor neuron growth and repair*. *Nature Neuroscience*, 2019. 22(2): p. 167-179.
43. Yun, S.-W., et al., *Neural stem cell specific fluorescent chemical probe binding to FABP7*. *Proceedings of the National Academy of Sciences*, 2012. 109(26): p. 10214-10217.
44. Gerstner, J.R., et al., *Brain fatty acid binding protein (Fabp7) is diurnally regulated in astrocytes and hippocampal granule cell precursors in adult rodent brain*. *PLoS One*, 2008. 3(2): p. e1631.
45. Butovsky, O. and H.L. Weiner, *Microglial signatures and their role in health and disease*. *Nature Reviews Neuroscience*, 2018. 19(10): p. 622-635.
46. Bachiller, S., et al., *Microglia in Neurological Diseases: A Road Map to Brain-Disease Dependent-Inflammatory Response*. *Frontiers in Cellular Neuroscience*, 2018. 12(488).
47. Allen, N.J. and C. Eroglu, *Cell Biology of Astrocyte-Synapse Interactions*. *Neuron*, 2017. 96(3): p. 697-708.
48. Hughes, A.N. and B. Appel, *Oligodendrocytes express synaptic proteins that modulate myelin sheath formation*. *Nature Communications*, 2019. 10(1): p. 4125.
49. Dzhashiashvili, Y., et al., *Nodes of Ranvier and axon initial segments are ankyrin G-dependent domains that assemble by distinct mechanisms*. *J Cell Biol*, 2007. 177(5): p. 857-70.

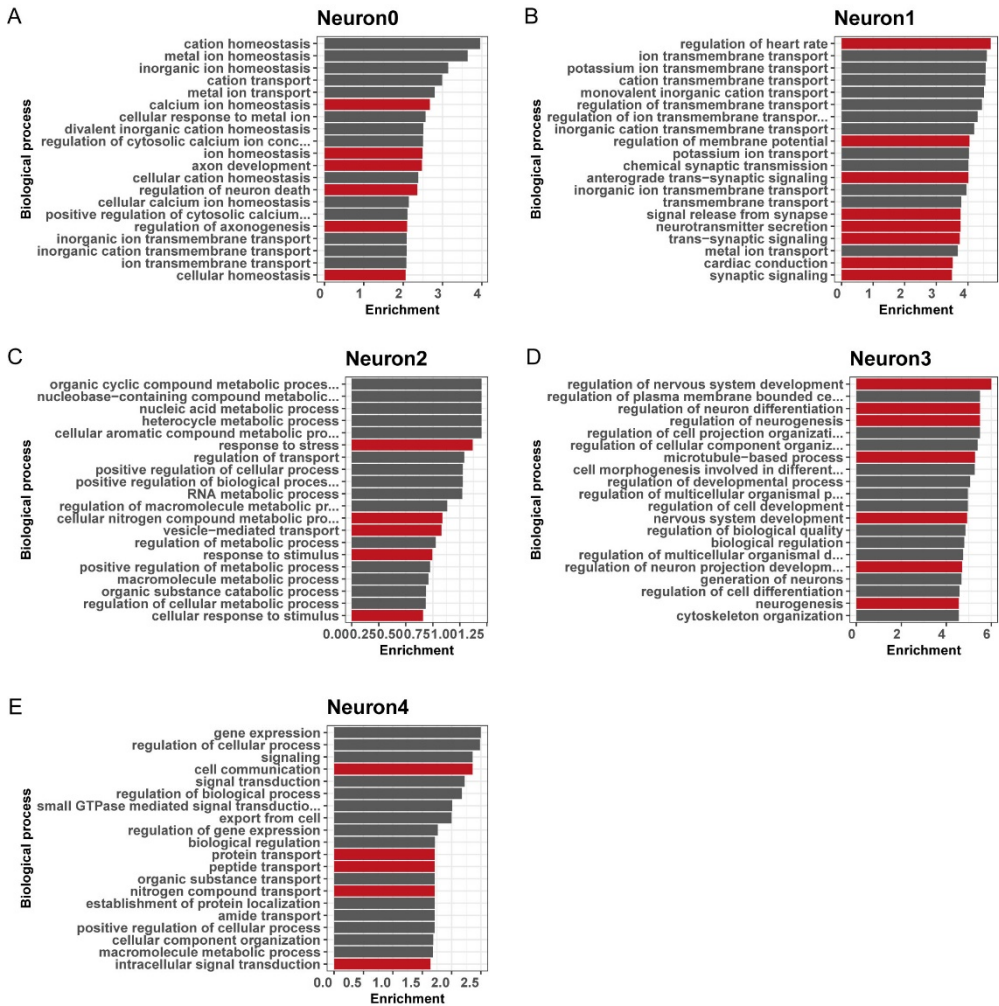
SUPPLEMENTAL FIGURES



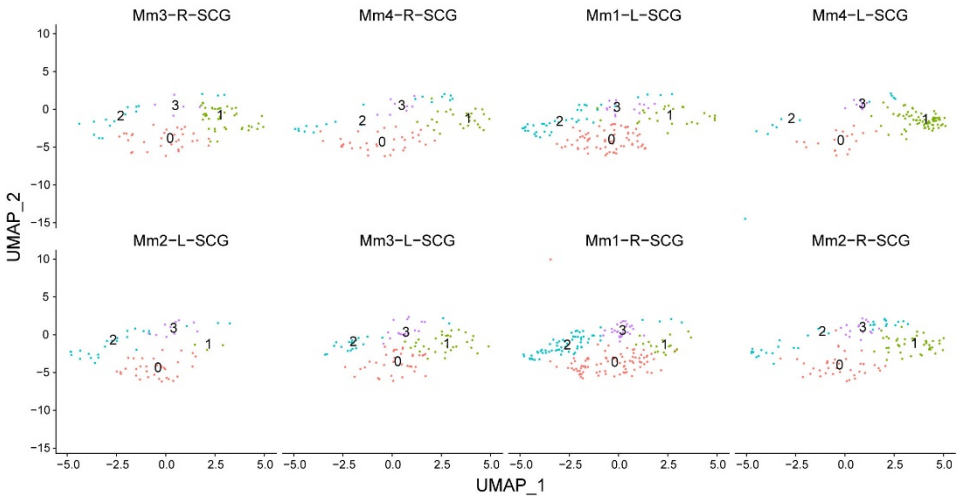
Supplemental Figure 1. Single nuclei clustering segregation and marker gene expression. A. Heatmap of top 10 DEGs of each cluster in mouse SCG showing the distinct gene expression patterns among clusters. B. UMAP showing expression of genes characteristic for major cell types in mouse SCG. Dashed lines indicate the boundaries of each cluster.



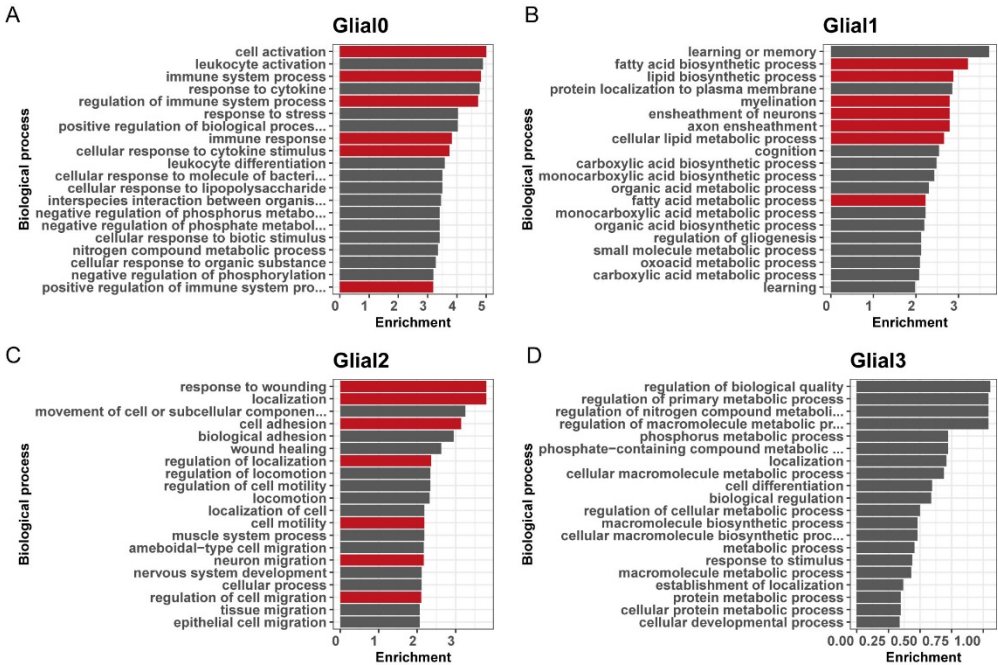
Supplemental Figure 2. UMAP plots of neuronal sub-clustering in eight individual samples.



Supplemental Figure 3. Glial cell subtype pathway identification. A-E. GO analysis of cellular subtypes (neuronal subcluster 0-4) in mouse SCG. Top 20 enriched biological process terms are shown.



Supplemental Figure 4. UMAP plots of satellite glial cell sub-clustering in eight individual samples.



Supplemental Figure 5. Glial cell subtype pathway identification. A-D. GO analysis of cellular subtypes (glial subcluster 0-3) in mouse SCG. Top 20 enriched biological process terms are shown.

Supplemental Table 1. DEGs of all clusters in mouse SCG

cluster	p_val	avg_log2FC	pct.1 (the specific cluster)	pct.2(the remaining clusters)	p_val_adj	gene
0	5,58E-251	1,155186	0,998	0,888	1,80E-246	Jun
0	8,96E-229	1,031058	0,997	0,863	2,89E-224	Junb
0	8,20E-223	0,990578	0,997	0,843	2,65E-218	Egr1
0	6,80E-221	0,959515	0,998	0,895	2,20E-216	Fos
0	1,14E-213	1,198485	0,937	0,572	3,67E-209	Zfp36
0	3,56E-203	1,146808	0,918	0,551	1,15E-198	Socs3
0	5,72E-193	1,229066	0,882	0,513	1,85E-188	Irf1
0	6,17E-182	1,123039	0,936	0,622	1,99E-177	Ccn1
0	8,22E-182	1,645215	0,78	0,42	2,65E-177	Gadd45g
0	3,55E-178	1,374782	0,883	0,562	1,15E-173	Dnajb1
0	2,74E-173	1,151691	0,875	0,532	8,86E-169	Phlda1
0	2,53E-170	1,124138	0,931	0,671	8,18E-166	Cebpd
0	2,98E-170	1,083206	0,89	0,553	9,61E-166	H2-Q4
0	7,98E-160	1,315184	0,66	0,282	2,57E-155	Acot1
0	7,39E-154	1,025383	0,924	0,699	2,38E-149	Jmjd1c
0	4,35E-147	0,937521	0,788	0,393	1,41E-142	Nop58
0	2,70E-144	1,025688	0,926	0,693	8,71E-140	Mt1
0	1,63E-142	0,997645	0,971	0,854	5,26E-138	Hspa1b
0	1,80E-137	0,722827	0,999	0,994	5,82E-133	Apoe
0	1,82E-136	0,87159	0,677	0,272	5,87E-132	Egr2
1	4,22E-198	1,105106	0,966	0,606	1,36E-193	Mboat2
1	1,02E-194	0,911269	0,995	0,863	3,29E-190	Scd2

1	1,22E-189	1,129088	0,967	0,633	3,94E-185	Pmepa1
1	6,19E-168	0,952881	0,973	0,661	2,00E-163	Lpar1
1	5,64E-158	1,0126	0,938	0,561	1,82E-153	Ptprz1
1	1,21E-154	0,829092	0,989	0,816	3,91E-150	Qk
1	6,49E-152	0,943986	0,876	0,46	2,09E-147	Mmd2
1	5,46E-140	0,909348	0,972	0,702	1,76E-135	Scd1
1	3,08E-139	1,107847	0,981	0,746	9,93E-135	Fabp7
1	1,26E-136	0,772041	0,995	0,821	4,08E-132	Abca8a
1	2,84E-134	1,064059	0,88	0,509	9,18E-130	Slc4a4
1	3,63E-134	0,871611	0,954	0,69	1,17E-129	Ptn
1	3,38E-132	0,944397	0,899	0,563	1,09E-127	Mapre2
1	1,64E-127	0,961361	0,818	0,44	5,31E-123	Tspan18
1	1,31E-126	1,003404	0,858	0,494	4,22E-122	Col28a1
1	3,71E-126	0,753898	0,996	0,9	1,20E-121	Dbi
1	4,25E-126	0,96837	0,901	0,544	1,37E-121	Lgr4
1	1,04E-125	0,848611	0,911	0,521	3,36E-121	Ttyh1
1	5,80E-124	0,744506	0,986	0,804	1,87E-119	Ncam1
1	4,80E-123	0,971833	0,743	0,342	1,55E-118	Grid1
2	1,08E-280	2,164069	0,521	0,065	3,48E-276	Ntrk3
2	2,10E-238	1,709265	0,943	0,693	6,77E-234	Ank3
2	1,94E-233	1,979247	0,867	0,495	6,27E-229	Scn7a
2	4,97E-185	1,687359	0,772	0,4	1,61E-180	Kcna1
2	1,16E-170	2,090916	0,82	0,519	3,76E-166	Cadm2
2	5,25E-139	1,210694	0,939	0,745	1,69E-134	Cdh19
2	3,66E-129	1,017289	0,973	0,808	1,18E-124	Nkain2

Single-nucleus RNA sequencing of murine SCG

2	3,45E-126	1,634771	0,366	0,079	1,11E-121	Flnc
2	1,88E-122	1,221902	0,963	0,85	6,09E-118	Stard13
2	5,30E-122	1,6946	0,589	0,237	1,71E-117	Emp1
2	1,40E-118	0,968883	0,924	0,836	4,53E-114	Utrn
2	1,67E-114	1,54439	0,476	0,158	5,39E-110	Fgl2
2	6,16E-96	1,295345	0,71	0,461	1,99E-91	lqgap2
2	5,29E-90	1,051097	0,826	0,627	1,71E-85	Zfp536
2	1,50E-78	0,929312	0,902	0,781	4,85E-74	Zswim6
2	1,25E-74	1,119485	0,829	0,666	4,04E-70	Pcdh9
2	5,17E-73	1,161342	0,599	0,352	1,67E-68	Hbegf
2	2,28E-72	0,616814	0,983	0,932	7,35E-68	Dst
2	1,51E-69	0,968401	0,851	0,746	4,88E-65	Fosb
2	3,21E-69	0,747687	0,901	0,767	1,04E-64	Chl1
3	8,18E-62	0,969157	0,961	0,918	2,64E-57	Dbi
3	8,37E-50	0,962317	1	0,996	2,70E-45	Apoe
3	5,49E-36	0,428216	1	1	1,77E-31	Gm42418
3	1,59E-33	0,914624	0,886	0,789	5,12E-29	Fabp7
3	7,38E-33	0,562599	0,986	0,991	2,38E-28	Cmss1
3	3,66E-27	0,757622	0,878	0,868	1,18E-22	Cst3
3	8,72E-27	0,832419	0,8	0,799	2,81E-22	Ckb
3	5,53E-26	0,510104	0,992	0,996	1,78E-21	AY036118
3	1,47E-22	0,575833	0,869	0,898	4,76E-18	Fth1
3	5,09E-22	0,656334	0,811	0,817	1,64E-17	mt-Co1
3	2,34E-20	0,642612	0,839	0,89	7,56E-16	Tuba1a
3	1,81E-19	0,550096	0,892	0,913	5,86E-15	Tmsb4x

3	1,85E-19	0,625355	0,861	0,823	5,99E-15	Atp1a2
3	4,55E-19	0,765657	0,814	0,857	1,47E-14	mt-Co3
3	8,64E-19	0,563014	0,897	0,891	2,79E-14	Scd2
3	1,61E-18	0,478728	0,917	0,944	5,21E-14	Cd9
3	1,44E-16	0,693519	0,8	0,763	4,66E-12	Mt1
3	9,35E-16	0,564472	0,803	0,867	3,02E-11	Rplp1
3	3,10E-15	0,702077	0,719	0,712	1,00E-10	Fads2
3	7,55E-15	0,508344	0,919	0,972	2,44E-10	Ubb
4	0	4,726438	0,95	0,062	0	Smoc2
4	0	4,049333	0,882	0,044	0	Lum
4	0	3,909641	0,676	0,032	0	Gfpt2
4	0	3,691319	0,857	0,034	0	Gpc3
4	0	3,595781	0,803	0,03	0	Ebf2
4	0	3,335434	0,84	0,052	0	Crispld2
4	0	3,194692	0,803	0,066	0	Col1a1
4	0	3,146537	0,748	0,011	0	Egfr
4	0	3,12974	0,773	0,031	0	Inpp4b
4	0	2,977498	0,718	0,023	0	Ccl11
4	0	2,942344	0,739	0,047	0	Ror1
4	0	2,901629	0,668	0,009	0	Pdgfra
4	0	2,686553	0,714	0,048	0	Pid1
4	0	2,597557	0,731	0,044	0	Vit
4	0	2,375251	0,639	0,024	0	Tgfb1
4	0	2,256682	0,664	0,021	0	Bnc2
4	0	2,241282	0,571	0,01	0	Scara5

Single-nucleus RNA sequencing of murine SCG

4	0	2,224234	0,538	0,017	0	Steap4
4	2,90E-300	2,343071	0,462	0,012	9,38E-296	Myoc
4	2,66E-299	2,839869	0,782	0,066	8,57E-295	Abi3bp
5	0	5,128264	0,995	0,039	0	Flt1
5	0	4,516822	0,946	0,026	0	Cypr1
5	0	3,957327	0,955	0,05	0	Pecam1
5	0	3,600954	0,936	0,017	0	Prkch
5	0	3,593843	0,941	0,049	0	Eng
5	0	3,559848	0,886	0,022	0	Mecom
5	0	3,516593	0,842	0,012	0	Gm20663
5	0	3,404249	0,906	0,017	0	Adgrl4
5	0	3,376597	0,906	0,031	0	Ptprb
5	0	3,371025	0,941	0,018	0	Adgrf5
5	0	3,123947	0,678	0,031	0	Slco2a1
5	0	3,120217	0,866	0,027	0	Emcn
5	0	3,082306	0,891	0,017	0	Cdh5
5	0	2,967538	0,743	0,04	0	Cxcl12
5	0	2,904818	0,842	0,015	0	Shank3
5	0	2,902043	0,891	0,021	0	Fli1
5	0	2,851468	0,886	0,039	0	Podxl
5	0	2,804952	0,866	0,019	0	Kdr
5	0	2,778672	0,847	0,042	0	Slfn5
5	0	2,626263	0,748	0,016	0	Cdh13
6	1,80E-116	4,918355	0,314	0,02	5,82E-112	Gm10801
6	1,19E-103	4,720511	0,298	0,021	3,84E-99	Gm10800

Chapter 7

6	6,55E-62	2,022162	1	1	2,11E-57	Gm42418
6	3,53E-60	2,080351	0,859	0,458	1,14E-55	Stmn2
6	4,04E-58	1,861813	0,937	0,702	1,30E-53	Uchl1
6	2,56E-56	1,805287	0,869	0,51	8,28E-52	Prph
6	7,29E-56	1,762126	0,874	0,494	2,35E-51	Tubb3
6	8,63E-56	1,832048	0,665	0,231	2,79E-51	Ndrq4
6	1,17E-54	1,549535	0,476	0,112	3,78E-50	Pirt
6	1,75E-53	1,499952	0,995	0,996	5,66E-49	AY036118
6	3,94E-53	1,387789	1	0,99	1,27E-48	Cmss1
6	6,68E-51	1,471733	0,555	0,161	2,16E-46	Basp1
6	5,14E-50	1,898765	0,958	0,804	1,66E-45	Map1b
6	6,26E-50	2,153109	0,901	0,637	2,02E-45	Slc6a2
6	3,79E-49	1,757346	0,764	0,355	1,22E-44	Cyb561
6	6,61E-49	1,601678	0,518	0,147	2,13E-44	Rab3c
6	2,68E-48	1,743264	0,806	0,441	8,65E-44	Pcsk1n
6	2,00E-47	1,747337	0,707	0,297	6,47E-43	Syt4
6	3,83E-46	1,539747	0,775	0,382	1,24E-41	Syt1
6	1,74E-44	1,492519	0,607	0,218	5,62E-40	Bex2
7	0	2,77176	0,808	0,027	0	Gm26871
7	0	2,761974	0,856	0,041	0	Erc2
7	0	2,533693	0,784	0,023	0	9530059014Rik
7	0	2,507673	0,848	0,041	0	Gpr158
7	0	2,47224	0,872	0,038	0	Ptpn2
7	0	2,438466	0,728	0,018	0	C130073E24Rik
7	0	2,335411	0,792	0,025	0	Kcnb2

Single-nucleus RNA sequencing of murine SCG

7	0	2,175881	0,712	0,024	0	Shisa9
7	0	2,109083	0,784	0,027	0	Hs3st5
7	0	1,786868	0,536	0,008	0	Gm20642
7	0	1,742581	0,48	0,004	0	Nrg3os
7	0	1,641719	0,448	0,004	0	Gm45321
7	0	1,266802	0,36	0,001	0	Gm2516
7	0	1,265201	0,456	0,004	0	4930587E11Rik
7	0	1,238337	0,464	0,004	0	Gm45323
7	3,67E-303	1,729972	0,496	0,008	1,19E-298	Gm13963
7	7,12E-303	0,973718	0,424	0,005	2,30E-298	Timp4
7	3,00E-297	2,71025	0,84	0,043	9,69E-293	Cacna2d3
7	8,54E-293	1,759724	0,688	0,025	2,76E-288	Srrm4
7	1,18E-290	3,025272	0,88	0,051	3,81E-286	Ryr2
8	0	3,496526	0,703	0,01	0	Myh11
8	0	3,311048	0,625	0,009	0	Abcc9
8	0	3,239672	0,672	0,011	0	Ano1
8	0	2,311215	0,547	0,003	0	Mrvi1
8	5,62E-230	1,452957	0,391	0,004	1,82E-225	Des
8	7,90E-228	1,821674	0,406	0,005	2,55E-223	Ndufa4l2
8	1,16E-220	3,388257	0,828	0,033	3,74E-216	Notch3
8	1,23E-213	5,259622	0,906	0,044	3,96E-209	Rgs5
8	2,19E-212	1,209482	0,328	0,003	7,08E-208	Aoc3
8	3,99E-206	3,037071	0,422	0,006	1,29E-201	Acta2
8	5,56E-182	1,804938	0,359	0,005	1,79E-177	Kcnj8
8	7,85E-158	2,013145	0,469	0,013	2,53E-153	Sdc1

8	5,26E-156	1,746464	0,406	0,009	1,70E-151	Cap2
8	2,99E-151	1,459359	0,328	0,005	9,65E-147	Angpt1
8	7,36E-146	2,165652	0,547	0,021	2,38E-141	Gm17276
8	1,21E-144	3,016445	0,5	0,017	3,90E-140	Cacnb2
8	1,89E-136	2,612237	0,406	0,011	6,10E-132	Trpc3
8	1,24E-126	2,076352	0,391	0,011	4,00E-122	Ngf
8	3,94E-118	2,922934	0,547	0,027	1,27E-113	Rgs6
8	1,08E-117	2,076446	0,391	0,012	3,49E-113	Lin7a
9	0	2,819295	0,739	0,008	0	Cldn1
9	0	2,32761	0,739	0,009	0	Ildr2
9	0	1,557562	0,522	0,002	0	Stra6
9	0	1,520011	0,435	0,001	0	Slc6a13
9	0	1,305872	0,413	0,001	0	Lypd2
9	2,90E-291	0,936488	0,304	0	9,36E-287	Mpzl2
9	7,49E-283	2,888788	0,826	0,016	2,42E-278	Thbs4
9	7,75E-268	2,057361	0,717	0,012	2,50E-263	Lbp
9	1,77E-186	1,566679	0,457	0,007	5,72E-182	Moxd1
9	8,75E-186	5,044909	0,978	0,044	2,82E-181	Bnc2
9	4,61E-177	3,223915	0,87	0,034	1,49E-172	Stxbp6
9	1,41E-173	2,595863	0,87	0,035	4,56E-169	Lmo7
9	4,30E-173	2,124606	0,674	0,019	1,39E-168	Mfap5
9	5,26E-170	5,045211	0,957	0,048	1,70E-165	Igfbp6
9	3,50E-155	1,376672	0,326	0,004	1,13E-150	Fbln1
9	2,49E-151	1,629242	0,435	0,008	8,05E-147	Col4a3
9	8,65E-145	2,665384	0,674	0,025	2,79E-140	Itgbl1

9	7,73E-144	1,00449	0,37	0,006	2,49E-139	Omd
9	2,88E-140	1,998228	0,587	0,018	9,30E-136	Cfh
9	4,19E-134	3,06093	0,826	0,044	1,35E-129	Klf5
10	0	3,929504	0,744	0,002	0	Cd86
10	0	3,673243	0,698	0,004	0	Rbm47
10	0	3,528198	0,767	0,001	0	Mir142hg
10	0	3,387477	0,512	0,001	0	Blnk
10	0	3,034705	0,605	0,002	0	Ptprc
10	0	2,63694	0,535	0,001	0	Nlrp3
10	0	2,383334	0,488	0,003	0	C1qa
10	0	2,296911	0,488	0,002	0	Spi1
10	0	2,158548	0,442	0,001	0	Lilrb4a
10	0	1,991559	0,419	0,001	0	C1qc
10	5,89E-300	2,353846	0,488	0,003	1,90E-295	C1qb
10	1,44E-299	2,007822	0,488	0,003	4,66E-295	Laptm5
10	3,71E-292	1,766681	0,326	0	1,20E-287	Gm30489
10	1,99E-291	2,892125	0,488	0,003	6,43E-287	Lyz2
10	5,17E-288	1,867723	0,302	0	1,67E-283	Lilr4b
10	7,56E-283	3,355917	0,605	0,007	2,44E-278	Pik3ap1
10	1,06E-274	1,768351	0,395	0,002	3,43E-270	Ikzf1
10	1,54E-268	1,481916	0,302	0	4,98E-264	Cd53
10	2,08E-268	2,543725	0,442	0,003	6,73E-264	Syk
10	8,17E-263	3,500216	0,535	0,005	2,64E-258	Mrc1
11	1,38E-214	2,541152	0,389	0,003	4,44E-210	Gldn
11	1,17E-200	2,619507	0,472	0,005	3,79E-196	Ncmap

11	2,38E-186	2,012751	0,333	0,002	7,68E-182	B230206H07Rik
11	5,67E-150	1,41521	0,278	0,002	1,83E-145	Cldn19
11	3,57E-114	1,542084	0,306	0,004	1,15E-109	Fa2h
11	4,12E-106	2,463933	0,611	0,023	1,33E-101	Bcas1
11	9,19E-92	2,233328	0,5	0,018	2,97E-87	Arhgap19
11	1,32E-88	2,889457	0,528	0,021	4,27E-84	Drp2
11	1,10E-74	1,840785	0,361	0,011	3,54E-70	Dusp15
11	2,74E-74	2,929182	0,639	0,038	8,85E-70	Stxbp6
11	2,94E-71	1,98468	0,306	0,008	9,50E-67	Emid1
11	1,01E-69	2,24402	0,444	0,019	3,27E-65	Ugt8a
11	8,61E-67	1,988055	0,333	0,01	2,78E-62	Plip
11	4,07E-60	2,711392	0,75	0,07	1,32E-55	Nfasc
11	3,21E-49	3,456207	0,778	0,098	1,03E-44	Prx
11	2,15E-47	4,567284	0,944	0,17	6,93E-43	Ctnna3
11	1,09E-46	1,990057	0,361	0,019	3,52E-42	Gm15541
11	2,89E-44	2,124599	0,333	0,017	9,32E-40	Mlip
11	9,10E-44	3,075827	0,667	0,075	2,94E-39	Lrrtm3
11	4,69E-40	2,329292	0,472	0,039	1,52E-35	Gm16168



